Eur. Phys. J. B **69**, 147–153 (2009)
DOI: 10.1140/epjb/e2009-00070-2

THE EUROPEAN PHYSICAL JOURNAL B

Regular Article

Stochastic resonance on paced genetic regulatory small-world networks: effects of asymmetric potentials

M. Perc[a]

Department of Physics, Faculty of Natural Sciences and Mathematics, University of Maribor Koroška cesta 160, 2000 Maribor, Slovenia

Received 22 October 2008 / Received in final form 9 December 2008
Published online 3 March 2009 –

Abstract. We study the phenomenon of stochastic resonance on small-world networks consisting of bistable genetic regulatory units, whereby the external subthreshold periodic forcing is introduced as a pacemaker trying to impose its rhythm on the whole network through the single unit to which it is introduced. Without the addition of additive spatiotemporal noise, however, the whole network remains forever trapped in one of the two stable steady states of the local dynamics. We show that the correlation between the frequency of subthreshold pacemaker activity and the response of the network is resonantly dependent on the intensity of additive noise. The reported pacemaker driven stochastic resonance depends significantly on the asymmetry of the two potential wells characterizing the bistable dynamics, which can be tuned via a single system parameter. In particular, we show that the ratio between the clustering coefficient and the characteristic path length is a suitable quantity defining the ability of a small-world network to facilitate the outreach of the pacemaker-emitted subthreshold rhythm, but only if the asymmetry between the potentials is practically negligible. In case of substantially asymmetric potentials the impact of the small-world topology is less profound and cannot warrant an enhancement of stochastic resonance by units that are located far from the pacemaker.

PACS. 05.40.-a Fluctuation phenomena, random processes, noise, and Brownian motion – 05.45.-a Nonlinear dynamics and chaos – 87.16.A- Theory, modeling, and simulations – 89.75.Hc Networks and genealogical trees

1 Introduction

Stochastic resonance [1] was introduced as a possible mechanism for the recurring occurrence of ice ages [2] and has since been established as an important phenomenon throughout natural sciences. Within the seminal works stochastic resonance was reported for bistable systems [3–5], but subsequently excitability [6] and proximity to special bifurcation points [7–9], especially in the context of related coherence resonance [10–14], have received substantial attention as well. Moreover, insights obtained for individual dynamical systems were latter on generalized for coupled systems [15–19], notably spatiotemporal stochastic resonance and spiral waves were first presented in [20], and eventually non-trivial effects of noise, such as array-enhanced stochastic [21] and coherence resonance [22], diversity induced resonance [23], and system size resonance [24,25] have been reported. Effects of noise on spatially extended systems have recently been reviewed in [26].

Complex networks [27] have also been identified as important entities influencing noise induced phenomena in nonlinear systems. Both stochastic [28,29] and coherence [30–32] resonance phenomena were already studied in networks with small-world topology [33,34], as were pattern formation and spatial order of spiral waves [35,36]. Stochastic resonance has also been reported on scale-free networks for coupled threshold elements [37] and the Ising model [38]. Recently an interesting study about the amplification of weak signals on scale-free networks of bistable oscillators has been published [39], and slightly earlier insightful findings regarding the synchronization on complex networks have been presented [40–42].

Our goal presently is to extend the subject by studying the stochastic resonance phenomenon on small-world networks in the presence of localized weak rhythmic activity only, whereby we use a bistable genetic regulatory model [43] as the underlying dynamical system. Various sources of stochasticity in genetic regulatory mechanisms have thus far been identified [44,45], but foremost it is the relatively small number of molecules constituting processes of gene expression that gives the strongest noisy component [46–48]. Besides experimental studies, theoretical analyses confirmed that the impact of noise on genetic regulatory models is significant and worthy of further

[a] e-mail: matjaz.perc@uni-mb.si

investigations [49,50]. From a more technical point of view, the presently used genetic regulatory model has a tuneable asymmetry of the bistable potential that can be adjusted via a single parameter, which makes it a good candidate for investigating the importance of such an asymmetry. Notably, the impact of asymmetric potentials on stochastic resonance has been researched in the past [51–54], and in general, a detrimental effect on stochastic resonance due to the asymmetry has been reported. Here we examine the possibility of stochastic resonance on paced small-world networks where the constitutive units have either a practically symmetric bistable potential or an asymmetric one. We show that the correlation between the periodic driving and the response of the system depends resonantly on the noise intensity, whereby the detailed impact of the small-world topology varies substantially in dependence on the asymmetry of the bistable potential. Namely, there exists an optimal fraction of rewired links, determined by the clustering coefficient and the characteristic path length of the underlying small-world network, at which the noise-induced spreading of pacemaker activity is pronounced best if the potential is symmetric. However, this feature is absent in case of an asymmetric bistable potential. We thus contribute to the existing literature studying the impact of pacemakers, which are isolated units in the system that dictate neighboring units the operating rhythm, on extended nonlinear dynamical systems [55–61].

The paper is structured as follows. In Section 2 we describe the genetic regulatory model and basic characteristics of its dynamics, as well as the considered small-world networks and other mathematical methods presently in use. Results are presented in Section 3, and in the last Section we summarize the results and briefly comment on the applicability of our findings.

2 Mathematical model and setup

The genetic regulatory model to be used presently was presented by Smolen et al. [43], and incorporates signal activated transcription and positive feedback on the rate of the transcriptional activator x. Due to the minimalist nature, the model can be described by a single ordinary differential equation of the form

$$\frac{dx_i}{dt} = \frac{\alpha x_i^2}{x_i^2 + H} - \kappa x_i + \beta + \sum_j \varepsilon_{ij}(x_j - x_i) + \sqrt{2D}\xi_i(t), \quad (1)$$

whereby the last two terms account for the coupling amongst the units and additive noise, respectively. Note that ε_{ij} is the coupling strength and $2D$ is the variance of Gaussian noise with zero mean and autocorrelation $\langle \xi_i(t)\xi_j(t')\rangle = \delta_{ij}\delta(t-t')$. Furthermore, α and κ are the saturation and degradation rate, respectively, H the dissociation constant, and β the basal synthesis rate of x. For further details about the model we refer the reader to the original work [43], while here we proceed by presenting some of its basic dynamical characteristics. Throughout this work we will, for simplicity, consider all quantities

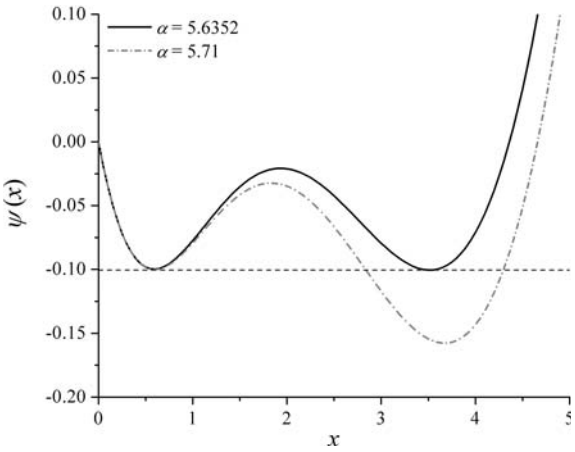

Fig. 1. Potential $\psi(x)$ of a single genetic regulatory unit for two different values of the saturation rate α in dependence on x. At $\alpha = 5.6352$ the bistable potential is practically symmetric, as additionally emphasized by the horizontal dashed line, whereas for $\alpha = 5.71$ the asymmetry is pronounced markedly.

as dimensionless and treat $H = 10$, $\kappa = 1$, $\beta = 0.4$ and $\varepsilon_{ij} = \varepsilon = 0.4$ as constants, whereas α and D will vary. If we introduce $\dot{x} = -\partial\psi(x)/\partial x$, and omit the coupling, the noise terms as well as the index i from equation (1), the potential function of an individual unit $\psi(x)$ can be written explicitly as

$$\psi(x) = -\alpha x + \alpha\sqrt{H}\arctan\left(x/\sqrt{H}\right) + \kappa x^2/2 - \beta x. \quad (2)$$

The outlay of $\psi(x)$ is depicted in Figure 1 for two different values of α. It can be observed that for $\alpha = 5.6352$ the bistable potential is practically symmetric, whereas for $\alpha = 5.71$ the asymmetry is pronounced markedly. Note that for $\alpha = 5.6352$ the symmetry is not perfect, yet the depth of both wells is the same (see horizontal dashed line in Fig. 1); hence we often refer to the potential as being practically symmetric. Thus, each constitutive unit of the network to be introduced below is characterized by two stable steady states, and depending on α, the potential wells characterizing them are either symmetric or asymmetric. The two cases depicted in Figure 1 will be studied separately in the next section.

To explore the possibility of stochastic resonance, we introduce a subthreshold pacemaker of the form $f_r(t) = A\cos(\omega t)$ to a single genetic regulatory unit $i = r$ of the network, which remains exposed to the periodic forcing during the whole simulation period. Throughout this study we use $A = 0.08$ and $\omega = \pi/300$, which warrant that in the absence of noise ($D = 0$) the pacemaker is subthreshold, meaning it cannot by itself induce transitions between the two stable steady states; not by the unit which is directly exposed and neither by any other constitutive unit of the network. However, small-amplitude intra-well motion is evoked even if $D = 0$, yet this does not significantly influence the main stochastic resonance phenomenon reported below.

Moreover, we consider small-world networks constituting the interactions amongst coupled units, which we obtain via the procedure described in [33] by starting from a

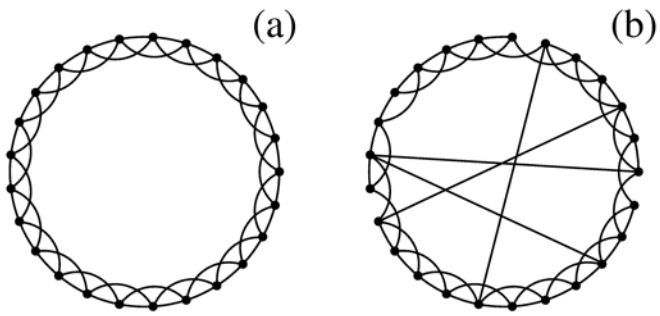

Fig. 2. Examples of considered network topologies. For clarity regarding k and p only 25 vertices are displayed in each panel. (a) Regular ring characterized by $p = 0$ with periodic boundary conditions. Each vertex is connected to its $k = 4$ nearest neighbors. (b) Realization of small-world topology via random rewiring of a certain fraction p of links (in this case 4 out of all 100 were rewired, hence $p = 0.04$).

regular ring with periodic boundary conditions, comprising $N = 200$ vertices each having connectivity $k = 4$, as shown in Figure 2a. In this scheme each vertex (or unit) corresponds to one noise driven bistable genetic regulatory unit. The probability of rewiring a link is denoted by p and can occupy any value from the unit interval, whereby $p = 0$ constitutes a regular graph while $p = 1$ results in a random network. For $0 < p < 1$, as exemplified in Figure 2b, the resulting network may have small-world properties in that the normalized characteristic path length L between distant units is small, i.e. comparable with that of a random network, while the normalized clustering coefficient C is still large, i.e. comparable with that of a regular nearest-neighbor graph constituting diffusive interactions amongst coupled units. According to [33], the characteristic path length is defined as the average number of edges in the shortest path between any two vertices, while the clustering coefficient is the average fraction of all $k_i(k_i - 1)/2$ allowable edges that actually exist amongst vertex i and all its k_i neighbors. Note that by small-world networks the degree inhomogeneity follows a Poissonian distribution (in the limit $p \to 1$) that is presently centered around $k = 4$, and thus due to their relative statistical homogeneity, especially if compared to networks with a scale-free degree distribution, the particular placing of the pacemaker within such networks is not crucial. If by a given value of p vertices i and j are connected then $\varepsilon_{ij} = \varepsilon_{ji} = \varepsilon$ but otherwise $\varepsilon_{ij} = \varepsilon_{ji} = \varepsilon_{ii} = 0$ in equation (1). It is worth noting that the average degree of the network, presently equaling $k_{avg} = 4$, is not affected by p and therefore the normalization of ε_{ij} with k_{avg} in equation (1) does not yield qualitatively different results (we could simply use $\varepsilon \to k_{avg}\varepsilon$).

Finally, for each set of the three main parameters α, D and p the temporal output of each unit is recorded for $N_T = 1000$ periods of the pacemaker, and the correlation of each series with the frequency of the pacemaker $\omega = 2\pi/T$ is computed via the Fourier coefficients $Q_i = \sqrt{R_i^2 + S_i^2}$ according to:

$$R_i = \frac{2}{TN_T} \int_0^{TN_T} x_i \sin(\omega t) dt,$$

$$S_i = \frac{2}{TN_T} \int_0^{TN_T} x_i \cos(\omega t) dt. \quad (3)$$

Since the Fourier coefficients are proportional to the square of the spectral power amplification, we presently use Q_i as the measure for stochastic resonance. To evaluate the response of the whole network by different D, the average of Q_i over all oscillators, defined as $S = N^{-1} \sum Q_i$, will be used. Importantly, the final results presented in the figures below were obtained by averaging Q_i over 100 different realizations of small-world configurations and initial conditions for each set of parameters to account for the inherent stochasticity that underlies the generation of such complex networks.

3 Results

We start by presenting Q_i in dependence on D and i by different α and p. Figure 3 features the resulting color maps for increasing values of p from top to the bottom panel. First we focus on the $\alpha = 5.6352$ case (left column in Fig. 3), which is characterized by a practically symmetric potential, as demonstrated in Figure 1. Clearly, there exist an optimal value of D by which the response of the network is optimally correlated with the localized subthreshold periodic forcing, thus indicating stochastic resonance in the examined system. Although the stochastic resonance phenomenon is better expressed for units that are in the immediate proximity of $i = r = 100$ that is under the direct influence of the pacemaker, the fine-tuning of p has the ability to optimally facilitate the outreach of the localized subthreshold periodic forcing. In particular, by $p = 0.16$ all units of the network feature the best expressed bell-shaped dependence of their respective Q_i on D, while by smaller and larger p this feature deteriorates substantially. Dashed lines on the left-hand side in the appropriate panel additionally mark this feature, although a clearer graphical presentation will be given below. Results presented in Figure 3 hence indicate that, besides an optimal D, there also exists an optimal small-world topology for the transmission of localized rhythmic activity across a noisy array of bistable genetic regulatory units with a symmetric potential. Panels on the right-hand side of Figure 3, on the other hand, while still showing signs of stochastic resonance, do not depict a similar dependence of Q_i on p. Indeed, it seems that in case of an asymmetric potential given by $\alpha = 5.71$ (see Fig. 1) the network topology is mostly of secondary importance, in particular since the color maps on the right of Figure 3 show very little deviation from top to bottom.

To study the above-outlined features more precisely, and to give a better quantitative view of presented results, we examine characteristic cross-sections of above

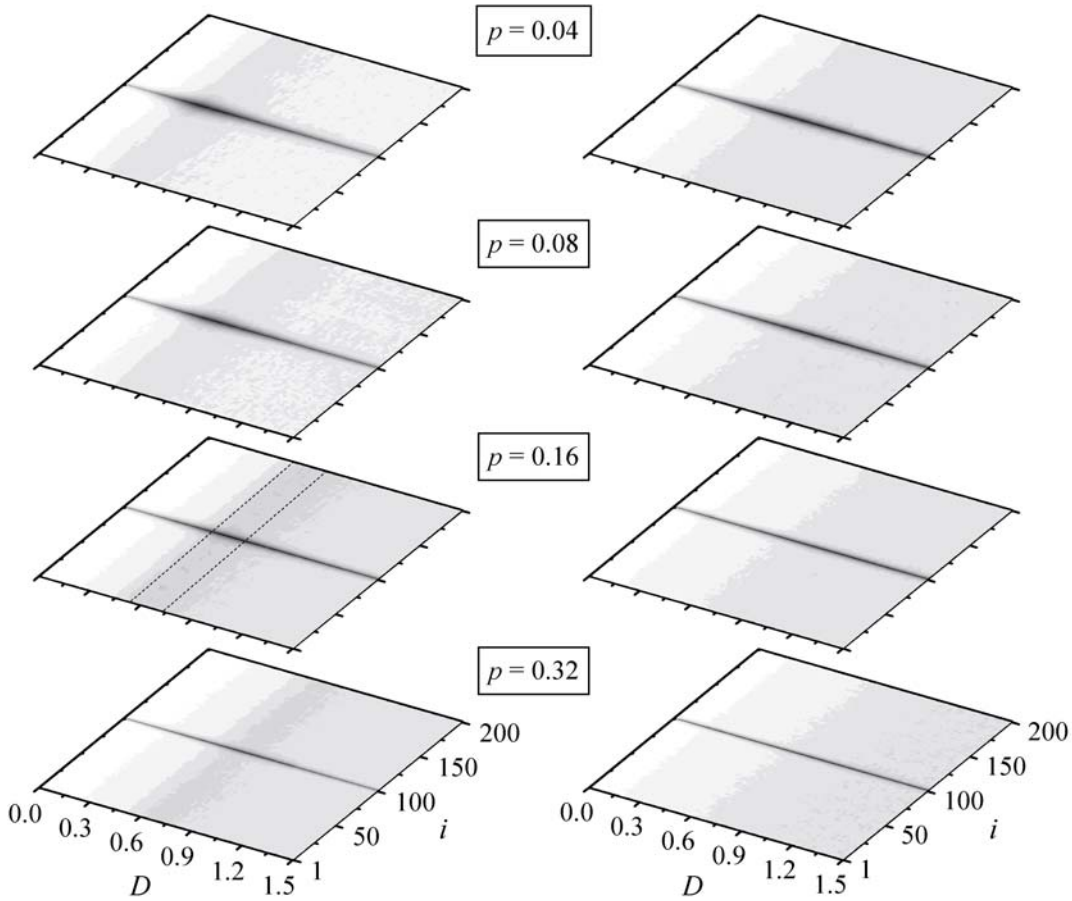

Fig. 3. (Color online) Color-coded Q_i in dependence on D and i for different p, obtained if $\alpha = 5.6352$ (left column) and $\alpha = 5.71$ (right column). In all panels the pacemaker has been introduced to the middle oscillator $i = r = 100$ and the color profile is linear, white marking minimal and black maximal values of Q_i. The intervals of Q_i from top to bottom left are: 0.0–0.076, 0.0–0.065, 0.0–0.056, 0.0–0.048; and the intervals from top to bottom right are: 0.0–0.058, 0.0–0.052, 0.0–0.046, 0.0–0.043. Note that the maximum of Q_i decreases continuously as p increases irrespective of α, and that the asymmetric potential (right column) yields lower maxima by a given value of p if compared to the practically symmetric case (left column). Moreover, $Q_{i=r}$ does not drop exactly to zero for $D = 0$ (note that the gray shading extends across the whole span of D) since the periodicity through the driven periodic responses within a potential well has not been subtracted.

color maps. Figure 4 features cross sections for $\alpha = 5.6352$. Panel (a) shows Q_i in dependence on D only for the oscillator that is under the direct influence of the pacemaker. This is the unit of the network by which the most correlated response with respect to the subthreshold periodic driving sets in, and accordingly, the overall maximal Q_i is obtained. It can be observed that the optimal D increases continuously as p increases, and simultaneously, the peak values of Q_i decrease. This decrease is related to the spread of the pacemaker impact to more distant units of the network, which is triggered by the additional shortcut links. Indeed, Figure 4b showing Q_i across the array for the optimal D, confirms this reasoning as the optimal $p = 0.16$ warrants notably higher Q_i especially for the units that are relatively far from $i = r = 100$. However, this feature is bounded with respect to p since both higher and lower values fail to deliver the same enhancement of Q_i across the whole array. Thus, there exists and optimal p that warrants the best outreach of the localized rhythmic activity to distant units (distant from the location of the pacemaker). This fact is additionally demonstrated in Figure 4c, where the overall network response S (the average over all Q_i by a given D) obtained for $p = 0.16$ shows a clear enhancement if compared to $p = 0.08$ and $p = 0.32$. Nevertheless, the increase in Q_i by units far from the pacemaker (see Fig. 4b) still cannot make fully up for the simultaneous decrease in Q_i by the unit (and its immediate neighbors) that is under the direct influence of the pacemaker (see Fig. 4a), and thus the overall maximal S is obtained by $p = 0.04$. In terms of the response of distant units, however, $p = 0.16$ gives the optimal small-world topology.

Before explaining the impact of different values of p on the stochastic resonance in case the bistable potential

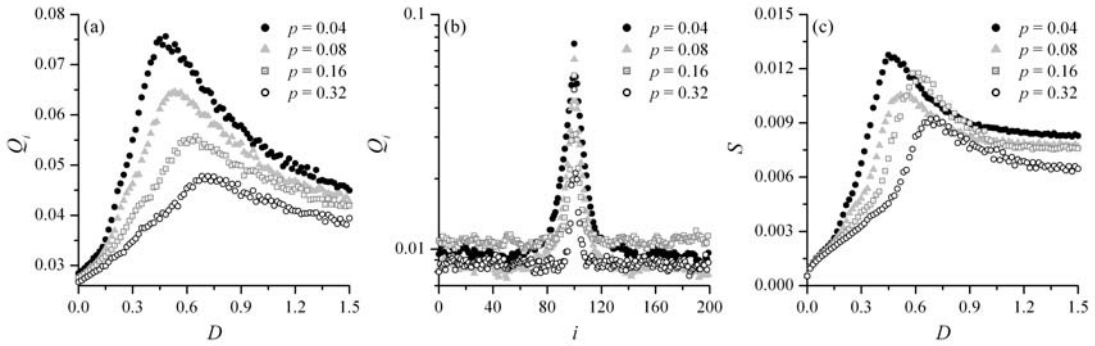

Fig. 4. (Color online) Characteristic cross-sections of color maps presented in the left column ($\alpha = 5.6352$; practically symmetric bistable potential) of Figure 3. Panel (a): Q_i in dependence on D for the oscillator $i = r = 100$ that is under the direct influence of the pacemaker. Panel (b): Q_i in dependence on i by the value of D warranting the peak S by a given p in the panel (c). Panel (c): S (response of the whole network; see Sect. 2) in dependence on D. Error bars in all panels equal maximally two times the height of symbols in up and down directions from the depicted data points.

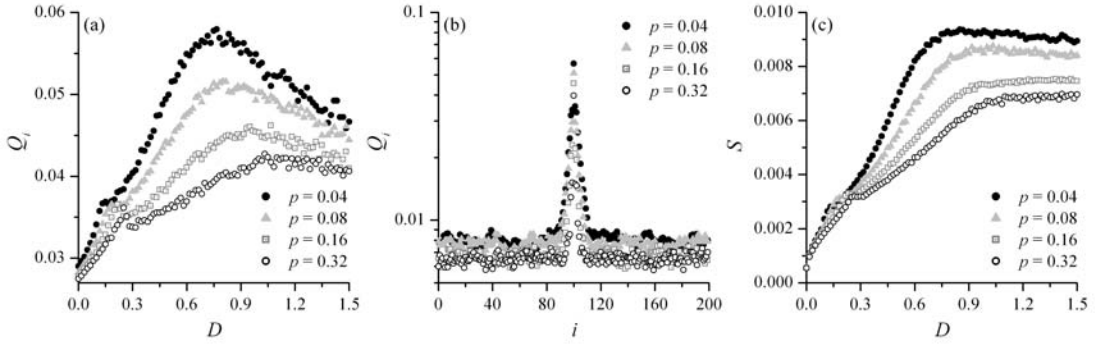

Fig. 5. (Color online) Characteristic cross-sections of color maps presented in the right column ($\alpha = 5.71$; asymmetric bistable potential) of Figure 3. Panel (a): Q_i in dependence on D for the oscillator $i = r = 100$ that is under the direct influence of the pacemaker. Panel (b): Q_i in dependence on i by the value of D warranting the peak S by a given p in the panel (c). Panel (c): S (response of the whole network; see Sect. 2) in dependence on D. Error bars in all panels equal maximally two times the height of symbols in up and down directions from the depicted data points.

is symmetric, we examine also the results obtained for $\alpha = 5.71$, yielding a notably asymmetric bistable potential. Figure 5 presents cross sections of color maps presented in the right column of Figure 3. As in Figure 4a, results for the unit that is directly perturbed by the pacemaker indicate that the optimal D increases and the peak values of Q_i decrease continuously as p increases. However, unlike by the $\alpha = 5.6352$ case, here this decrease is not accompanied by a notable increase of Q_i by the units that are far from the pacemaker. In fact, results presented in Figure 5b show that Q_i by the remote units decrease also as p increases. Both these features of the two cross sections depicted in panels (a) and (b) manifest clearly also in the overall network response, which decreases steadily as additional shortcuts replace nearest-neighbor links (see Fig. 5c). This leads to the conclusion that asymmetric bistable potentials are not susceptible for an enhancement of pacemaker-driven stochastic resonance via the fine-tuning of small-world topology, and that indeed strictly diffusive interactions in such a case might constitute an optimal interaction topology. Moreover, it can be observed that in Figure 5c the peaks of S are broader and lower than in Figure 4c, which is also a consequence of the asymmetric potential that might play a significant role in deteriorating the phenomenon of stochastic resonance [51].

Worthy of notice, the asymmetric bistable potential does evoke an additional feature that can be observed for small D in Figure 5a (and partially also in panel (c)). Namely, the so-called subharmonic stochastic resonance peak evoked by small D mainly by the unit that is directly paced and its immediate neighbors, similarly as reported previously in [5]. Presently, however, this feature is not of foremost importance but solely supplements the array of phenomena that can be observed if small-world networks of asymmetric bistable units are weakly paced and driven by additive noise.

Finally, aiming to explain the existence of the above-established optimal small-world topology for the symmetric potential, we employ classical measures such as the normalized characteristic path length L and the normalized clustering coefficient C [33], as defined in Section 2. While L is often the more appraised quantity (echoing in the name "small-world" describing such networks), the

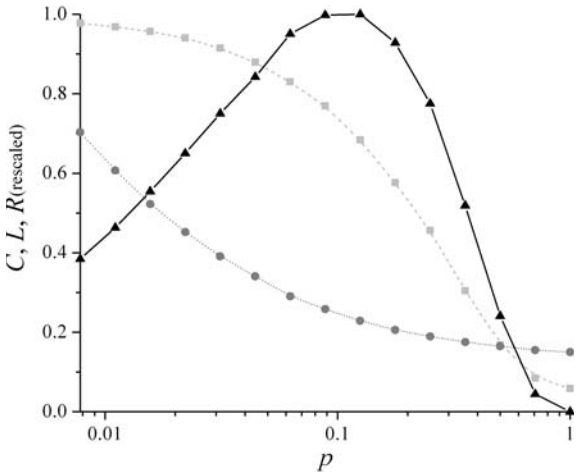

Fig. 6. (Color online) Normalized clustering coefficient C (squares), normalized characteristic path length L (circles), and the ratio $R = C/L$ (triangles) in dependence on p for a network consisting of $N = 200$ vertices having average connectivity $k = 4$. Results were averaged over 100 different realizations of each network, and the ratio R was rescaled to the unit interval (the shape of the dependence on p was completely preserved) for better comparisons of all three curves. Lines are solely guides to the eye, while error bars are smaller than the size of symbols of the depicted data points.

clustering coefficient is presently also crucial since it quantifies to what extend local interactions are intact or broken. In particular, $C = 1$ means that the cliquishness of nearest neighbors is perfect, while $C = 0$ means that the neighbors connected to a given unit of the network are disconnected from one another. Since the effectiveness of the pacemaker to transmit its rhythm also to units that are not within its immediate proximity relies both on effective nearest-neighbor interactions as well as on the ability to reach physically distant units towards which information might get lost via the diffusive route, we propose the ratio between the normalized clustering coefficient and the characteristic path length $R = C/L$ as the quantity defining the optimal properties of a network to facilitate the spreading of localized pacemaker-emitted rhythmic activity. The higher the value of R, the better the network structure is adapted to enforce the pacemaker activity on the distant units. A high value of R suggests that the nearest-neighbor interactions are largely intact, while at the same time considerable benefits in terms of information propagation may be expected from long-range connections. On the other hand, a low value of R indicates either that nearest-neighbor interactions are largely broken or that long-range connections are sparse, whereby any of these two properties would act detrimental on the ability of a pacemaker to enforce its rhythm on distant units of the network. Results for the presently employed network ($N = 200$, $k = 4$) are shown in Figure 6. Indeed, the peak value of R is obtained by roughly the same value of the small-world connectivity, equaling $p \approx 0.15$, that also warrants the best outreach of the pacemaker to units that are not in its immediate proximity. Importantly, in terms of the network structure $p \approx 0.15$ significantly shortens the path length between pairs of vertices (see circles in Fig. 6) while simultaneously keeping the clustering coefficient fairly high (see squares in Fig. 6), thus constituting the optimal network topology in terms of the ratio R as argued above. This result confirms our reasoning and introduces a compact measure for assessing the ability of a small-world network topology to promote the spreading of localized rhythmic activity to units that are located far from the pacemaker.

4 Summary

We study the phenomenon of stochastic resonance on genetic regulators small-world networks subject to a subthreshold periodic driving. If the potential characterizing the local dynamics is symmetric, the stochastic resonance in units that are far from the pacemaker can be enhanced by an appropriate small-world topology. Thereby the ratio between the clustering coefficient and the shortest path appears to be a suitable quantity for assessing the network's ability to facilitate the outreach of the pacemaker. On the other hand, if the potential is asymmetric, benefits from a carefully adjusted small-world topology cannot be expected, and thus diffusive interactions seem to be optimal. Notably, the subharmonic stochastic resonance, which is evoked by small noise intensities, can be observed provided the asymmetry is sufficiently pronounced. Due to the significant importance of pacemakers in various networks connecting natural systems [62–64], we hope our study will be applicable in realistic genetic regulatory experiments, and foster the understanding of processes by which weak pacemakers play a key role.

M. Perc acknowledges support from the Slovenian Research Agency (grant Z1-9629).

References

1. L. Gammaitoni, P. Hänggi, P. Jung, F. Marchesoni, Rev. Mod. Phys. **70**, 223 (1998)
2. C. Nicolis, G. Nicolis, Tellus **33**, 225 (1981)
3. R. Benzi, A. Sutera, A. Vulpiani, J. Phys. A **14**, L453 (1981)
4. L. Gammaitoni, F. Marchesoni, E. Menichella-Saetta, S. Santucci, Phys. Rev. Lett. **62**, 349 (1989)
5. P. Jung, P. Hänggi, Phys. Rev. A **44**, 8032 (1991)
6. A. Longtin, J. Stat. Phys. **70**, 309 (1993)
7. A. Neiman, P.I. Saparin, L. Stone, Phys. Rev. E **56**, 270 (1997)
8. A.F. Rozenfeld, C.J. Tessone, E. Albano, H.S. Wio, Phys. Lett. A **280**, 45 (2001)
9. O.V. Ushakov, H.-J. Wünsche, F. Henneberger, I.A. Khovanov, L. Schimansky-Geier, M.A. Zaks, Phys. Rev. Lett. **95**, 123903 (2005)
10. D. Sigeti, W. Horsthemke, J. Stat. Phys. **54**, 1217 (1989)
11. G. Hu, T. Ditzinger, C.Z. Ning, H. Haken, Phys. Rev. Lett. **71**, 807 (1993)

12. W.J. Rappel, S.H. Strogatz, Phys. Rev. E **50**, 3249 (1994)
13. A.S. Pikovsky, J. Kurths, Phys. Rev. Lett. **78**, 775 (1997)
14. A. Longtin, Phys. Rev. E **55**, 868 (1997)
15. P. Jung, U. Behn, E. Pantazelou, F. Moss, Phys. Rev. A **46**, R1709 (1992)
16. A.R. Bulsara, G. Schmera, Phys. Rev. E **47**, 3734 (1993)
17. H.S. Wio, Phys. Rev. E **54**, R3075 (1995)
18. A. Neiman, L. Schimansky-Geier, Phys. Lett. A **197**, 379 (1995)
19. H. Gang, H. Haken, X. Fagen, Phys. Rev. Lett. **77**, 1925 (1996)
20. P. Jung, G. Mayer-Kress, Phys. Rev. Lett. **74**, 2130 (1995)
21. J.F. Lindner, B.K. Meadows, W.L. Ditto, M.E. Inchiosa, A.R. Bulsara, Phys. Rev. Lett. **75**, 3 (1995)
22. C. Zhou, J. Kurths, B. Hu, Phys. Rev. Lett. **87**, 098101 (2001)
23. C.J. Tessone, C.R. Mirasso, R. Toral, J.D. Gunton, Phys. Rev. Lett. **97**, 194101 (2006)
24. P. Jung, J.W. Shuai, Europhys. Lett. **56**, 29 (2001)
25. G. Schmid, I. Goychuk, P. Hänggi, Europhys. Lett. **56**, 22 (2001)
26. F. Sagués, J.M. Sancho, J. García-Ojalvo, Rev. Mod. Phys. **79**, 829 (2007)
27. R. Albert, A.-L. Barabási, Rev. Mod. Phys. **74**, 47 (2002)
28. Z. Gao, B. Hu, G. Hu, Phys. Rev. E **65**, 016209 (2001)
29. H. Hong, B.J. Kim, M.Y. Choi, Phys. Rev. E **66**, 011107 (2002)
30. O. Kwon, H.-T. Moon, Phys. Lett. A **298**, 319 (2002)
31. O. Kwon, H.-H. Jo, H.-T. Moon, Phys. Rev. E **72**, 066121 (2005)
32. M. Özer, M. Uzuntarla, T. Kayikcioglu, L.J. Graham, Phys. Lett. A **372**, 6498 (2008)
33. D.J. Watts, S.H. Strogatz, Nature **393**, 440 (1998)
34. M.E.J. Newman, D.J. Watts, Phys. Lett. A **263**, 341 (1999)
35. D. He, G. Hu, M. Zhan, W. Ren, Z. Gao, Phys. Rev. E **65**, 055204(R) (2002)
36. M. Perc, New J. Phys. **7**, 252 (2005)
37. A. Krawiecki, Physica A **333**, 505 (2004)
38. A. Krawiecki, Int. J. Mod. Phys. B **18**, 1759 (2004)
39. J.A. Acebrón, S. Lozano, A. Arenas, Phys. Rev. Lett. **99**, 128701 (2007)
40. C. Zhou, J. Kurths, Phys. Rev. Lett. **96**, 164102 (2006)
41. A. Arenas, A. Diaz-Guilera, C.J. Perez-Vicente, Physica D **224**, 27 (2006)
42. C. Zhou, A.E. Motter, J. Kurths, Phys. Rev. Lett. **96**, 034101 (2006)
43. P. Smolen, D.A. Baxter, J.H. Byrne, Am. J. Physiol. Cell Physiol. **274**, 531 (1998)
44. W.J. Blake, M. Kærn, C.R. Cantor, J.J. Collins, Nature **422**, 633 (2003)
45. J. Paulsson, Nature **427**, 415 (2004)
46. H.H. McAdams, A. Arkin, Trends Genet. **15**, 65 (1999)
47. M.B. Elowitz, A.J. Levine, E.D. Siggia, P.S. Swain, Science **297**, 1183 (2002)
48. J.M. Pedraza, J. Paulsson, Science **319**, 339 (2008)
49. J. Hasty, D. McMillen, F. Isaacs, J.J. Collins, Nat. Rev. Genet. **2**, 268 (2001)
50. Z. Wang, Z. Hou, H. Xin, Chem. Phys. Lett. **401**, 307 (2005)
51. R. Bartussek, P. Hänggi, P. Jung, Phys. Rev. E **49**, 3930 (1994)
52. F. Chapeau-Blondeau, Phys. Rev. E **55**, 2016 (1997)
53. F. Marchesoni, F. Apostolico, S. Santucci, Phys. Rev. E **59**, 3958 (1999)
54. H.S. Wio, S. Bouzat, Braz. J. Phys. **29**, 136 (1999)
55. S. Alonso, I. Sendiña-Nadal, V. Pérez-Muñuzuri, J.M. Sancho, F. Sagués, Phys. Rev. Lett. **87**, 078302 (2001)
56. T.R. Chigwada, P. Parmananda, K. Showalter, Phys. Rev. Lett. **96**, 244101 (2006)
57. H. Kori, A.S. Mikhailov, Phys. Rev. Lett. **93**, 254101 (2004)
58. F. Radicchi, H. Meyer-Ortmanns, Phys. Rev. E **73**, 036218 (2006)
59. J. Steele, M. Tinsley, K. Showalter, Chaos **16**, 015110 (2006)
60. R. Zhang, L. Yang, A.M. Zhabotinsky, I.R. Epstein, Phys. Rev. E **76**, 016201 (2007)
61. M. Perc, Phys. Rev. E **76**, 066203 (2007)
62. A.M. Katz, *Physiology of the Heart* (Kluwer, Philadelphia, 2000)
63. R. Dumollard, J. Caroll, G. Dupont, C. Sardet, J. Cell. Sci. **115**, 3557 (2002)
64. R.E. Haddock, C.E. Hill, J. Physiol. **566**, 645 (2005)